On the anatomy of the air-gun signature

Halvor Groenaas, Ola Pramm Larsen, and David Gerez, WesternGeco; Matthew Padula, Teledyne Bolt*

Summary

In the context of designing a new air-gun with reduced high-frequency emissions, we developed computational fluid dynamics models that provide new insight into the dynamic behavior of air-guns. We combined these simulations with video images and high-fidelity acoustic measurements from physical tests to investigate the physical mechanisms contributing to the air-gun signature. We considered the dynamic output in the time domain, and the energy components in the frequency domain.

Introduction

Figure 1 shows a cross section of a typical air-gun. Before firing, the forces exerted by the pressurized air in the operating chamber and the fire chamber act on the two faces of the shuttle to keep it in the sealed position. When the solenoid valve is actuated by an electrical signal it initiates an air flow that shifts the net force, accelerating the shuttle to the right. This exposes a progressively larger area of the ports, allowing air to escape from the fire chamber into the surrounding water.

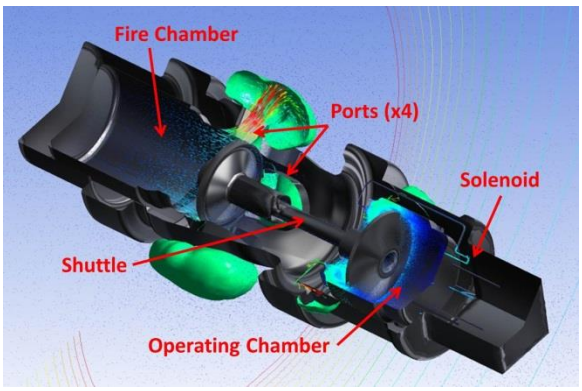

Figure 1: Internal components of an air-gun. The fire chamber is sealed with the shuttle in its left-most position.

Rayleigh's (1917) description of the period of collapse of a cavity in water is the foundation of early analytical models of air-gun signatures, which were validated with experimental results. Giles et al. (1973) described the output of arrays comprised of air-guns that individually produced spherical and non-interacting bubbles. Ziolkowski et al. (1982) and Vaage et al. (1984) considered the interactions among multiple spherical bubbles. Laws et al. (1990) generalized the equations to include the behavior of clusters. Cox et al. (2004) then considered the effects of non-spherical bubble geometries. To address growing concerns about the potential environmental effects of high-frequency noise, Landrø et al. (2011) investigated mechanisms that could generate such noise, such as ghost cavitation and mechanical clicking.

We used advanced computational fluid dynamics (CFD) models to describe the physical mechanisms behind the air-gun signature, and validated these models against experimental results. We performed this work in the context of designing a new air-gun with reduced high-frequency emissions, described by Coste et al. (2014) and Gerez et al. (2015).

Models and measurements

We first developed 3D CFD models to understand the dynamic interactions across multiple domains: fluid flows and pressures within the air-gun, mechanical displacements and forces, the stochastic oscillation of the air bubble, and the propagation of acoustic waves in the near-field. This presents a number of modeling challenges, including severe pressure gradients, sub-microsecond transient time steps, multiphase flows, and hexahedral dominant meshes of up to five million elements. We improved simulation efficiency by taking advantage of symmetry, emulating specific paths, configuring dynamic meshes, and optimizing time steps. Modeling inevitably involves a compromise between fidelity and execution time, so we developed a range of models tailored to specific tasks, with execution times ranging from 12 hours for our $^1/_8$-3D production model to several weeks for our full-3D maximum-fidelity model.

We then performed physical experiments with two objectives: calibration and validation. We used specially made air-guns fitted with Hall-effect motion sensors and multiple pressure transducers to measure internal parameters that we applied to calibrate the CFD model. We then acquired near- and far-field acoustic signatures with a calibrated high-frequency acquisition system, taking special measures to eliminate spurious noise and vibrations. We used these acoustic measurements to validate the model's predictions of the air-gun itself and the bubbles' interaction with the surrounding water. We calibrated and validated on a variety of designs, providing added confidence in the model's predictions across the entire design space.

We also recorded video imagery of a limited set of firing events with a high-speed camera capable of up to 3,000 frames per second. We used these images to qualitatively confirm that the model produces the expected bubble.

Figure 2 shows an example of validation for a single design point. There is an excellent agreement between the experimental (blue) and CFD (cyan) results for the new air-gun, in both the time and frequency domains. There is only a small difference in the precursor that precedes the main peak, caused by a difference in the internal geometries, but this does not have a significant effect on output energy. The standard air-gun (black) has a very different pulse shape and spectrum.

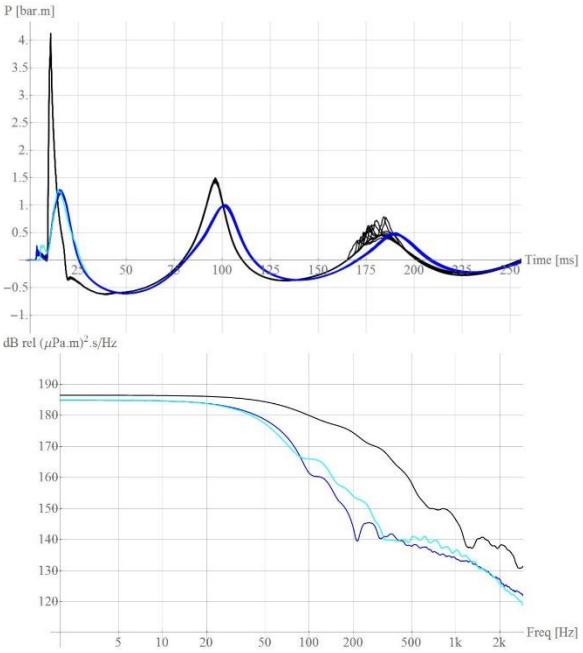

Figure 2: Signature of the new air-gun (configured for its most restrictive bandwidth and 150 cu. in.) as predicted by CFD (cyan) and as measured over 10 shots (blue); and measured signature of a standard air-gun (black) over 10 shots. Upper panel: time domain. Lower panel: frequency domain calculated over main peak.

The instrumented air-guns also allowed us to observe an interesting effect, unrelated to the validation objective. The small oscillations in the bubble train of the standard air-gun (black) are caused by the re-injection of air into the water as the shuttle repeatedly bounces, before coming to rest and sealing the fire chamber. The re-injection may be directly visible as extra peaks in the signature as in this case, or it may modulate the bubble train as air either reinforces or damps the bubble. Figure 3 (acquired during a different test), proves that the shuttle does indeed bounce in a standard air-gun. The new air-gun, by completely emptying the air in the fire chamber on the first stroke, prevents this phenomenon.

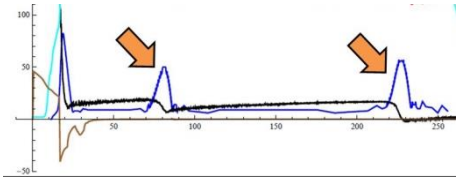

Figure 3: Measurements from sensors positioned inside an instrumented standard air-gun: Hall-effect shuttle-motion sensor (blue), fire-chamber pressure (black), and solenoid current (brown). Two secondary shuttle strokes (arrows) can be seen.

Decomposing the air-gun signature

Having validated the CFD model, we now decompose the air-gun signature into three main components: precursor, main peak, and free-bubble oscillation. We use CFD simulations and video images to understand the physical mechanisms, and examine their contributions to the measured output. We compare two air-guns: a standard air-gun, and the new air-gun in the most restrictive of its three bandwidth configurations.

Precursor

The precursor is a small-amplitude broadband event that precedes the main peak of the acoustic signature. We confirm that air flows represent the basic mechanism. As the shuttle starts to move, but before it reaches the ports, the fire-chamber seal is opened and pressurized air escapes through the small annular gap between the shuttle and the surrounding housing. The radial gap size of thousandths of an inch represents a tradeoff between minimizing acoustic noise, and preventing mechanical contact between moving parts that would cause wear and compromise reliability. This escaping air forms the precursor bubble, shown in the CFD simulation of Figure 4. The left inset of Figure 5 shows the precursor (red) produced by a standard air-gun in a physical experiment.

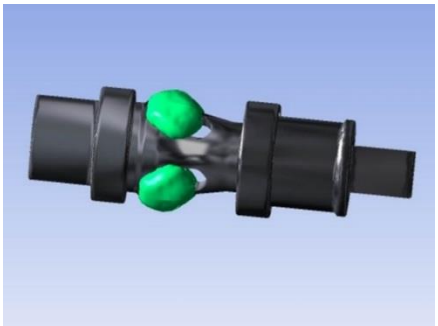

Figure 4: CFD simulation showing the precursor bubble immediately before the main release of air through the ports. At this stage the shuttle has just reached the beginning of the ports.

Main peak

The main peak is formed when the shuttle moves past the ports, allowing most of the air in the fire chamber to escape into the surrounding water. In a standard air-gun, the shuttle accelerates to a high speed before reaching the ports, resulting in the steeply rising flank of Figure 5 (green line, right inset). In contrast, the new air-gun releases air more gradually, resulting in a signature with a gentler slope and reduced peak amplitude (Figure 6). As the bubble expands, its motion is opposed by the local hydrostatic pressure and by the inertia of the surrounding water, reducing the rate of volume growth and the resulting acoustic pressure. The existing precursor bubble also affects the injection of the main bubble, typically damping the primary peak and reducing the amount of high-frequency energy.

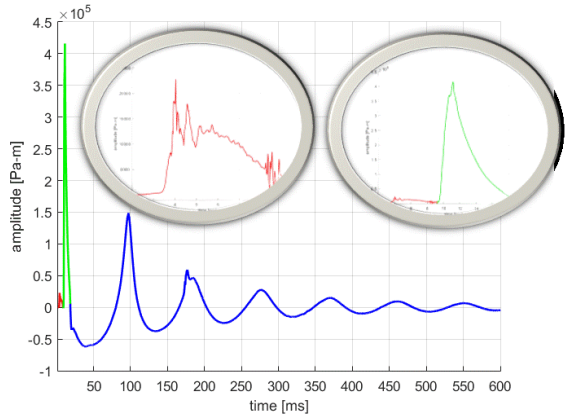

Figure 5: Measured signature of a standard 155 cu. in. air-gun, with close-up of the precursor (red) and main peak (green).

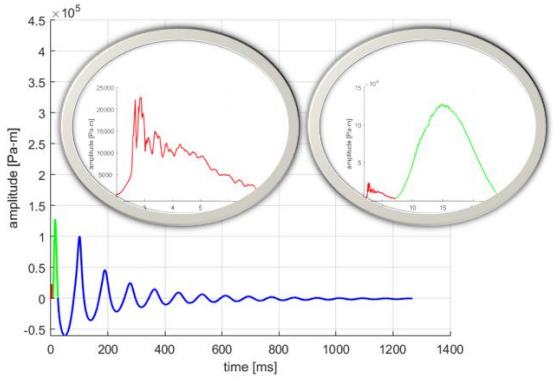

Figure 6: As Figure 5, but for the new air-gun at 150 cu. in.

Free-bubble oscillation

After the shuttle has re-sealed the ports, gun dynamics no longer directly influence the bubble. Nevertheless, the bubble retains a "memory" in the sense that the conditions during its initial release affect the subsequent series of compression and rarefaction cycles. The period of an instantaneously released bubble is essentially determined by two factors: the mass of air in the bubble, with more air producing a longer period; and the hydrostatic pressure, with higher pressure producing a shorter period. In addition, the state of the precursor bubble at the time of the primary release, and the rate of release, both directly affect the amplitude of the bubble train. Figure 5 (blue) shows the standard air-gun's bubble train. The new air-gun (Figure 6, blue) empties the fire chamber more effectively, resulting in bubble oscillations with a slightly longer period and higher relative amplitude. If the air-gun fails to release all of the air in the fire chamber on the first shuttle stroke, re-injection of air might affect the amplitude (reducing or increasing it depending on the timing) and period (with the larger mass of air producing a longer period).

Contributions to the amplitude spectrum

Next, we consider the frequency content of the signatures of the standard air-gun (Figure 7) and the new air-gun (Figure 8).

For both air-guns, we see that the precursor emits far less energy in the seismic band than the other two components. Its contribution is more pronounced at higher frequencies, albeit at a lower absolute level; these higher frequencies account for a negligible share of the energy emitted by an air-gun (Gerez et al., 2015).

The difference between the two air-guns is most pronounced in the main peak. The main peak clearly dominates the output of the standard air-gun above 40 Hz. For the new air-gun, it dominates over a narrow band from 40 to 150 Hz, above which the precursor is highest.

The freely oscillating bubble is the main source of energy below 40 Hz for both air-guns. Below the fundamental bubble frequency of approximately 10 Hz, the main peak and bubble appear to have *more* energy than the combined signature, but this is the result of signal-processing artifacts: DC spectral leakage artificially boosts main-peak energy in this region, and removing the destructive interference between the main peak and the bubble troughs boosts the bubble energy.

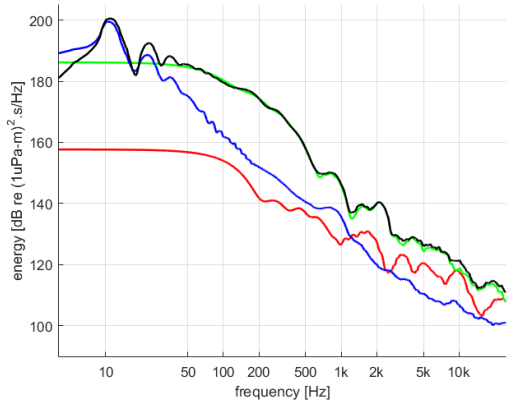

Figure 7: Decomposed amplitude spectrum of Figure 5 showing the contributions of the precursor (red), main peak (green) and free bubble (blue). The spectrum of the full signature is shown in black. The curves were generated by zero-padding the signature components, performing an FFT, and applying a one-third octave smoother.

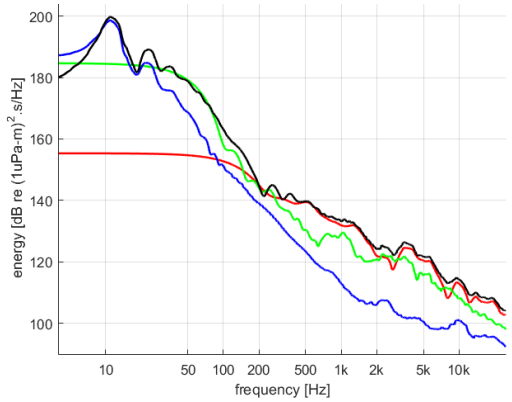

Figure 8: Decomposed amplitude spectrum of the new air-gun

Signature stability

Although air-gun output is remarkably stable in the seismic band, it is still subject to three main sources of variability: short-term shot variation, manufacturing tolerances, and normal long-term wear. We measured shot variation physically, with the high-frequency system described above. It would be impractical to physically characterize the remaining two sources of variation to a reasonable statistical confidence, or to simulate in CFD due to the long computation times. We therefore developed a statistical meta-model that can replace the CFD model in predicting the output spectrum, training the Kriging model (Sacks et al., 1989) by performing CFD simulations over the design space. We then used Monte Carlo methods to predict the expected range of the output as a result of random inputs.

In Figure 9, we see that the output is very stable in the seismic band. Absolute amplitudes are far lower at higher frequencies, so the relative variability is higher. This is a signal-to-noise issue: components of the signature that are inherently less stable (the precursor and high-frequency incoherent energy from the main peak) are relatively more pronounced in the output spectrum. Moreover, long-term wear increases the precursor size.

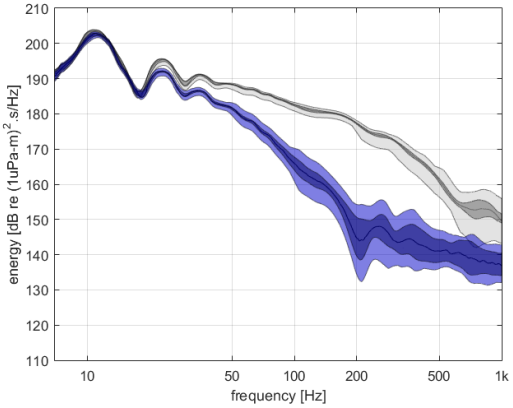

Figure 9: Expected range bands from shot variation for a standard air-gun (dark gray) and the new air-gun (dark blue); from manufacturing tolerances for a standard air-gun (light gray); and from the combination of manufacturing tolerances and long-term wear for the new air-gun (light blue).

Conclusions

We applied advanced CFD models and physical experiments to decompose the air-gun signature into its primary components. The air escaping through a mechanical gap produces a small precursor peak that contributes little overall energy. By increasing the rise time of the main pulse, we reduced the unwanted high-frequency noise. By simultaneously maximizing the amount of air released into the bubble, we increased the signal in the seismic band. Like any mechanical device, air-guns are subject to variability, and we characterized the output levels that can be expected for any given air-gun over its operating life.

Acknowledgments

In addition to the authors, many people have contributed to these results. Among them are: Emmanuel Coste, Jostein Farstad, Svein Huseboe, Jon-Fredrik Hopperstad, Robert Laws, Anneli Soppi, and Michel Wolfstirn.

EDITED REFERENCES

Note: This reference list is a copyedited version of the reference list submitted by the author. Reference lists for the 2016 SEG Technical Program Expanded Abstracts have been copyedited so that references provided with the online metadata for each paper will achieve a high degree of linking to cited sources that appear on the Web.

REFERENCES

Coste, E., D. Gerez, H. Groenaas, J.-F. Hopperstad, O.-P. Larsen, R. Laws, J. Norton, M. Padula, and M. Wolfstirn, 2014, Attenuated high-frequency emission from a new design of airgun: SEG Technical Program Expanded Abstracts, 132–137, http://dx.doi.org/10.1190/segam2014-0445.1.

Cox, E., A. Pearson, J. R. Blake, and S. R. Otto, 2004, Comparison of methods for modelling the behavior of bubbles produced by marine seismic airguns: Geophysical Prospecting, **52**, 461–477, http://dx.doi.org/10.1111/j.1365-2478.2004.00425.x.

Gerez, D., H. Groenaas, O. P. Larsen, M. Wolfstirn, and M. Padula, 2015, Controlling air-gun output to optimize seismic content while reducing unnecessary high-frequency emissions: 85th Annual International Meeting, SEG, Expanded Abstracts, 154–158, http://dx.doi.org/10.1190/segam2015-5843413.1.

Giles, B. F., and R. C. Johnston, 1973, System approach to air-gun array design: Geophysical Prospecting, **21**, 77–101, http://dx.doi.org/10.1111/j.1365-2478.1973.tb00016.x.

Landrø, M., L. Amundsen, and D. Barker, 2011, High-frequency signals from air-gun arrays: Geophysics, **76**, no. 4, Q19–Q27, http://dx.doi.org/10.1190/1.3590215.

Laws, R. M., L. Hatton, and M. Haartsen, 1990, Computer modelling of clustered airguns: First Break, **8**, 331–338, http://dx.doi.org/10.3997/1365-2397.1990017.

Rayleigh, O. M., 1917, On the pressure developed in a liquid during the collapse of a spherical cavity: Philosophical Magazine, **34**, 94–98, http://dx.doi.org/10.1080/14786440808635681.

Sacks, J., W. J. Welch, T. J. Mitchell, and H. P. Wynn, 1989, Design and analysis of computer experiments: Statistical Science, **4**, 409–423, http://dx.doi.org/10.1214/ss/1177012413.

Vaage, S., B. Ursin, and K. Haugland, 1984, Interaction between airguns: Geophysical Prospecting, **32**, 676–689, http://dx.doi.org/10.1111/j.1365-2478.1984.tb01713.x.

Ziolkowski, A., G. Parkes, L. Hatton, and T. Haugland, 1982, The signature of an air gun array: Computation from near-field measurements including interactions: Geophysics, **47**, 1413–1421, http://dx.doi.org/10.1190/1.1441289.